ACS EARTH AND SPACE CHEMISTRY

http://pubs.acs.org/journal/aesccq

Article

Vacuum Ultraviolet Photoionization of Methane-Water Clusters Leads to Methanol Formation

Published as part of ACS Earth and Space Chemistry special issue "Harold Linnartz Festschrift".

Nureshan Dias, Alexander K. Lemmens, Anna Wannenmacher, and Musahid Ahmed*

Cite This: *ACS Earth Space Chem.* 2024, 8, 1867−1876

Read Online

ACCESS | Metrics & More | Article Recommendations | Supporting Information

ABSTRACT: We report on the photoionization of a series of small methane-water mixed clusters generated in a supersonic jet expansion. The resulting clusters are investigated by synchrotron-based single photon vacuum ultraviolet (VUV) ionization coupled with reflectron time-of-flight mass spectrometry. Pure methane clusters $(CH_4)_n^+$ and protonated water clusters $(W_nH)^+$ dominate the mass spectra, however with judicious control of backing pressure and mixing ratio, mixed methane-water clusters are generated. We gain unique insights into the underlying dynamics and chemistry of methane and mixed methane-water clusters through the analysis of fragment mass spectra, and photoionization intensity curves, which provide appearance energies, which are then compared to theoretically calculated ionization energies. In particular, we provide experimental evidence of the formation of methanol upon photoionization of the mixed clusters under cold conditions, which is directly relevant to astrochemistry.

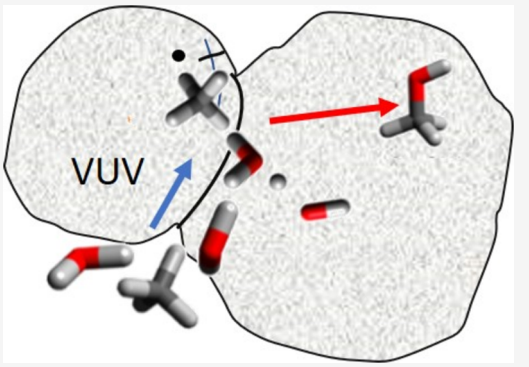

KEYWORDS: *molecular beams, astrochemistry, mass spectrometry, clathrates, density functional theory, ice, photochemistry*

INTRODUCTION

In planetary environments and astrochemical bodies, such as comets, icy planetary satellites, and Kuiper belt objects, and in the Interstellar Medium (ISM) (molecular clouds), methane (M) and water (W) emerge as abundant constituents, existing in both condensed and gaseous states. In our solar system, both methane and water have been detected on Earth, Mars, Triton, Eris, and Pluto.[1−6] Moreover, methane and water ice clouds are thought to be present in the atmosphere of Neptune and Uranus.[7,8] Within the interstellar medium, characterized by extreme cold, molecules accrete onto the surface of dust particles, giving rise to the formation of icy grain mantles. These interstellar ices exhibit two distinct phases: water-poor and water-rich, with the water-rich phase being primarily composed of water and CO_2, along with NH_3 and CH_4.[9] These astrochemical bodies are consistently exposed to ionizing radiation originating from stars and/or galactic cosmic rays. These molecules are also abundant in photodissociation regions of molecular clouds where it can be exposed to vacuum ultraviolet (VUV) radiation.[10] This exposure induces both chemical and physical modifications in the nascent ices, leading to the formation of various more complex chemical species.

On Earth, methane is one of the most potent greenhouse gases, and substantial quantities are sequestered in deposits on the deep ocean floor. In these high-pressure environments, water molecules form cage-like structures to enclose "guest" methane molecules, forming clathrates.[11] This structural arrangement enhances stability and acts as a natural mechanism to prevent excessive methane emissions, thereby significantly contributing to climate moderation.[12,13] There are reports indicating the existence of methane clathrates in the subsurface of Mars and Titan, suspected to continuously feed their atmospheres with methane.[14] Methane clathrates are also thought to form in the internal oceans of Enceladus and Europa, influencing their compositions.[14] However, despite theoretical predictions suggesting the formation of methane clathrates in the interstellar medium (ISM), their direct detection in these regions has proven to be elusive.

Previous studies on mixed methane and water clusters primarily comprise theoretical investigations aimed at understanding the formation of large methane clathrates and exploring the hydrogen bonding interactions between CH_4 and water molecules.[15−20] Salazar-Cano et al.,[21] in particular, found that the hydrogen bonding between water molecules

Received: May 21, 2024
Revised: August 1, 2024
Accepted: August 2, 2024
Published: August 9, 2024

strengthens within these mixed clusters when compared to isolated water dimers. Consequently, this results in a weakening of the hydrogen bonding between methane and water in mixed clusters, in contrast to CH_4-H_2O dimer.

There is a paucity of experimental information for methane-water clusters, in contrast to the theoretical results mentioned above. We note that Johnson, Fujii, and co-workers published a series of papers examining the messenger-tagged vibration photodissociation spectra of $Ar-CH_4-H_3O^+$,[22] $H^+(H_2O)_6$-CH_4,[23] and Ar-$(CH_4)_3$-H_3O^+.[24] However, the experiments most closely related to the methane-water cluster systems studied here arise from those that examine the photochemistry of methane-water ices. VUV photolysis of such ices results in the formation of diverse oxygenated hydrocarbons.[25] Notably, even with minimal water concentrations in methane ices, the analysis of infrared (IR) spectra demonstrated the efficient generation of alkanes and oxygen-bearing organics, including C_2H_6, C_2H_4, C_3H_8, H_2CO, CH_3CHO, CH_3OH, and more. The formation of alcohols like CH_3OH, CH_3CH_2OH, and $CH_3CH_3CH_2OH$ from CH_4, C_2H_6, and C_3H_8 can occur through two pathways involving either O or OH fragments derived from water.[25,26] Hodyss and colleagues[27] found that hydroxyl radicals, generated by the photolysis of water, play a dominant role in the photochemistry, oxidizing methane into CH_3OH, HCHO, CO, and ultimately CO_2. Recently, the New Horizons spacecraft investigations on the Kuiper Belt object Arrokoth revealed a significant presence of methanol ices along with various organic materials.[28] These observations suggest that the formation of these organic compounds may have occurred through the photolysis mechanisms discussed earlier.

The reports of rich chemistry in methane-water ices motivated this study of mixed methane-water clusters, which provides an excellent template to probe photochemistry at a molecular level under isolated, cold conditions, which is directly relevant to astrochemistry. We report on the structural motifs and photoionization dynamics of methane−water clusters using synchrotron-based VUV photoionization mass spectrometry measurements combined with continuous supersonic molecular beam expansion. We thereby provide experimental evidence of photochemistry that can occur within condensed phases of ubiquitous compounds in various planetary and interstellar environments.

EXPERIMENTAL SECTION

The experiments are performed in a continuous molecular beam apparatus coupled to a time-of-flight (TOF) mass spectrometer located at Beamline 9.0.2 at the Advanced Light Source.[29,30] Briefly, neutral clusters are supersonically expanded through a 50 μm nozzle with backing pressures exceeding 20 psi. The size distribution of clusters changes depending on the backing pressure. The gas expansion is skimmed by a 1 mm skimmer situated 15 mm downstream before interacting with the synchrotron radiation. The pressures in the source and interaction chambers are 4.2×10^{-4} and 1.4×10^{-5} Pa, respectively, under normal operating conditions. To obtain mixed clusters, a gas mixture containing various percentages of methane in argon is passed through a bubbler containing water. In the main chamber, the neutral cluster beam is interrogated in the ionization region of a Jordan reflectron time-of-flight (TOF) mass spectrometer by tunable VUV radiation. Since the synchrotron light is quasi-continuous (500 MHz), a start pulse for the TOF ion packet is provided by pulsing the ion optic electric potential. The extractor and repeller plates of the ion optics are biased at the same potential (1600 V), and ions are extracted by fast switching of the repeller plate to 1900 V with a pulse width of 2.5 μs. Ions are accelerated perpendicularly to their initial velocity direction through the field-free region toward the reflectron. Ions, reflected in the electrostatic field of the ion mirror, are detected by a microchannel plate (MCP) installed at the end of the second field-free region. The time-dependent electrical signal from the MCP is amplified by a fast preamplifier, collected by a multichannel-scalar card, and thereafter integrated with a PC computer. Time-of-flight spectra are recorded for the photon energy range between 10.5 and 14.5 eV with a 0.5 m/z mass resolution. The typical photon energy step size used for these experiments is 50 meV. The photoionization intensity curves of the clusters are obtained by integrating over the peaks in the mass spectrum at each photon energy and dividing by the photon flux. Deuterated methane and deuterated water, both separately and in combination, are utilized to elucidate and identify various species. During the course of all experiments described here, no unexpected or unusually high safety hazards were encountered.

COMPUTATIONAL DETAILS

Theoretical calculations were performed on a methane-water cluster system. A conformational search was performed using the semiempirical quantum chemistry package CREST.[31] The lowest energy conformer from this search was further geometry optimized, in both neutral and cationic states, using Q-Chem at the ωB97X-V/def2-TZVPPD level of theory.[32] Full optimization of the cationic states was performed to determine the adiabatic ionization energy, as well as visualize the ionized clusters in the molecular beam. Vertical ionization energies (VIE) for clusters were determined by performing single-point calculations on cations by using the optimized geometries of the neutral clusters. These single-point calculations were performed at the same level of theory (ωB97X-V/def2-TZVPPD) as the geometry optimization. The functional ωB97X-V contains nonlocal van der Waals correlation and so is well suited for noncovalent interactions such as those between methane and water.[33] The VIE of $(H_2O)(CH_4)_2$ was also calculated based on the structures reported by Riera et al.[34]

RESULTS

Figure 1 presents the mass spectra obtained while varying the backing pressures at a 13 eV photon energy for a mixture comprising 30% methane in argon (Ar). This allows us to observe the changes that occur in the size distribution of clusters. Lower backing pressure (30 psi) correlates with a higher amount of water-rich clusters but near-zero populations of mixed water and methane clusters (Figure 1a). In contrast, higher backing pressure (80 psi) leads to a reduced population of protonated water clusters but an increased population of methane-containing clusters, as shown in Figure 1c. Mixed methane-water clusters were found to be formed mostly under moderate pressure conditions (50 psi backing pressure), as depicted in Figure 1b.

A more detailed depiction of the mass spectra of mixed methane/water clusters (obtained at 65 psi backing pressure and 13 eV photon energy) is shown in Figure 2. Eight different cluster systems can be seen here. To identify these clusters the positive charge is placed at the end of the cluster species

https://doi.org/10.1021/acsearthspacechem.4c00151
ACS Earth Space Chem. 2024, 8, 1867−1876

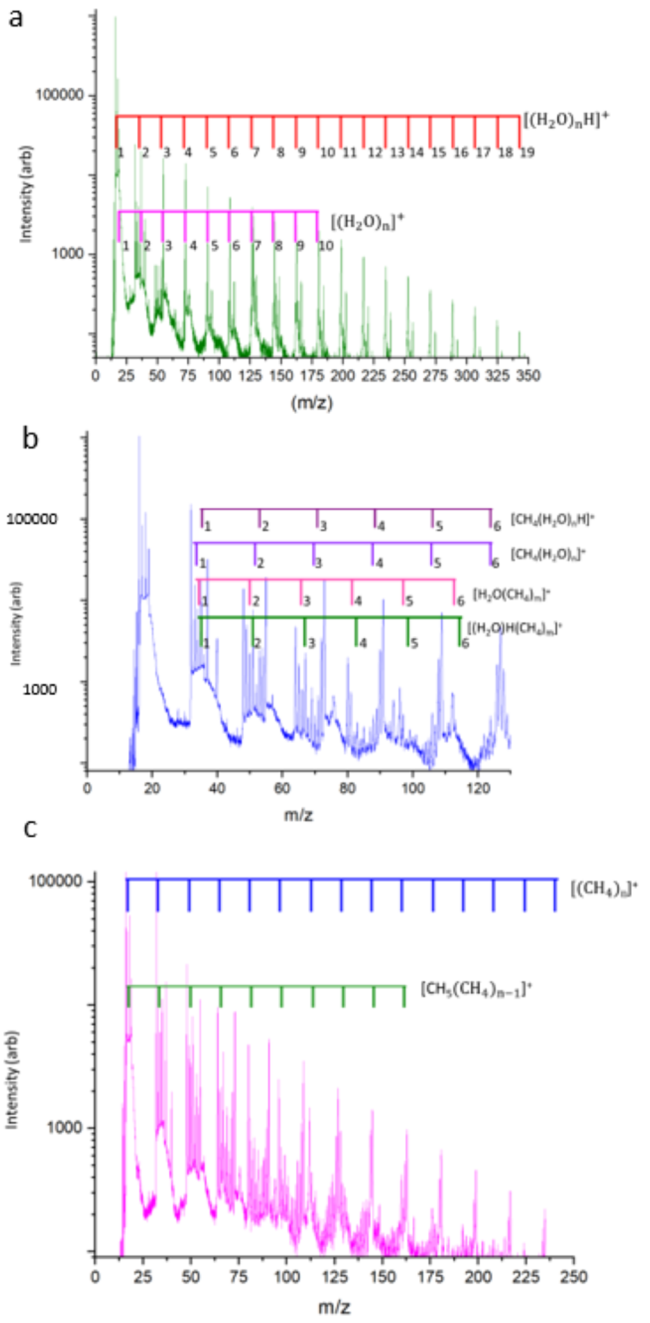

Figure 1. Mass spectra obtained at three different backing pressures (a) 30, (b) 50, and (c) 80 psi at a photon energy of 13 eV. The combs indicate cluster series measured in the experiment.

notation, as the exact location of the charge is not determined in our experiment. These clusters includes methane clusters $[(CH_4)_n]^+$ (m/z 16 and appears at every m/z 16 intervals, up to n = 16); protonated methane clusters $[CH_5(CH_4)_n]^+$ (first peak appears at m/z 33 for n = 1, and subsequently appears at every m/z 16 interval, up to n = 11); pure water clusters $[(W_m)]^+$ (first peak appears at m/z 18 for m = 1 and subsequently appears at every m/z 18 interval, up to m = 20); protonated water clusters $[(W)_mH]^+$ (first peak at m/z 19 for m = 1 and subsequently appears at every m/z 18 interval, up to m = 20); methane-water clusters $[CH_4(W)_m]^+$ (first peak appears at m/z 34 for m = 1 and subsequently appears at every m/z 18 interval, up to m = 14); methane-protonated water clusters $[CH_4(W)_mH]^+$ (first peak appears at m/z 35 for m = 1 and subsequently appears at every m/z 18 interval, up to m = 13); water–methane clusters $[W(CH_4)_n]^+$ (first peak appears at m/z 34 for n = 1 and subsequently appears at every m/z 16 interval, up to n = 13); water-protonated methane clusters $[(CH_4)_nWH]^+$ (first peak appears at m/z 35 and subsequently appears at every m/z 16 interval, up to n = 9). Figure 2b presents an enlarged version of the mass spectra within the range of 46–74 amu, highlighting predominantly the ternary (M_3, W_3, and clusters of the form M_2W or W_2M and the protonated form of them) and quaternary cluster series (clusters of the form M_4 W_4 and clusters of the form M_3W or W_3M and the protonated form of them).

Appearance Energies (AE) of Methane-Water Clusters. The photoionization intensity curves for each series of clusters measuring up to 5 or 6 subunits are presented in Figure S1 in the Supporting Information (SI), covering the 10.5–13.2 eV energy region. The appearance energies (AE) for each cluster are indicated by an arrow in the curve. The AE is obtained from the initial point above the baseline, after which the signal exhibits a progressively increasing trend. The (AE) of methane, water, water-dominated methane, and methane-dominated water clusters as well as the theoretically calculated vertical ionization energies (VIE) for the methane-dominated water and water-dominated methane (structures are shown in Figure S2 in the SI) are plotted against cluster size are shown in Figure 3. The AE and calculated VIE's of clusters observed in this study (up to 5 or 6 subunits) are shown in Table 1. The general trend in the AE's of pure water and methane clusters is a decrease in appearance energy with increasing cluster size. However, for the methane dimer, the observed AE is lower than expected. This deviation can be attributed to the presence of a small amount of an O_2 (AE = 12.07 eV) impurity in the molecular beam which shares the same mass as the methane dimer and influences the AE. Another anomaly is the apparent rise in the calculated VIE for $(H_2O)(CH_4)_2$ in contrast to what is observed in the experiments. This occurs for the geometry shown in Figure 3 where the water molecule is in a plane perpendicular to the two methane molecules. However, calculating the VIE in line with a recent structure reported by Riera et al.[34] where the oxygen in the water is pointed away from the two methane molecules leads to an VIE more in line with the trends observed in this work. The absolute energies calculated for the neutral structures lie very close to each other, with the difference being 0.015 kcal/mol. The AE's for the water-dominated mixed cluster follow those of pure water clusters. There is no apparent trend in the AE for methane-dominated mixed clusters.

DISCUSSION

Interpretation of Mass Spectra. *Pure Methane and Water Clusters.* The homogeneous clusters observed in this study are examined first. As depicted in Figure 1c, under ideal conditions, we observe clusters as high as $[(CH_4)_{20}]^+$. We anticipate that the photoionization of the relatively weakly bound methane clusters results in extensive dissociation, in the same way as observed by Ding et al.,[35] who conducted a study on ion–molecule reactions within methane clusters triggered by photoionization, yielding similar results to those observed in our study. The methane clusters that we discuss here would then have been mainly formed by the following reaction.[35]

https://doi.org/10.1021/acsearthspacechem.4c00151
ACS Earth Space Chem. 2024, 8, 1867–1876

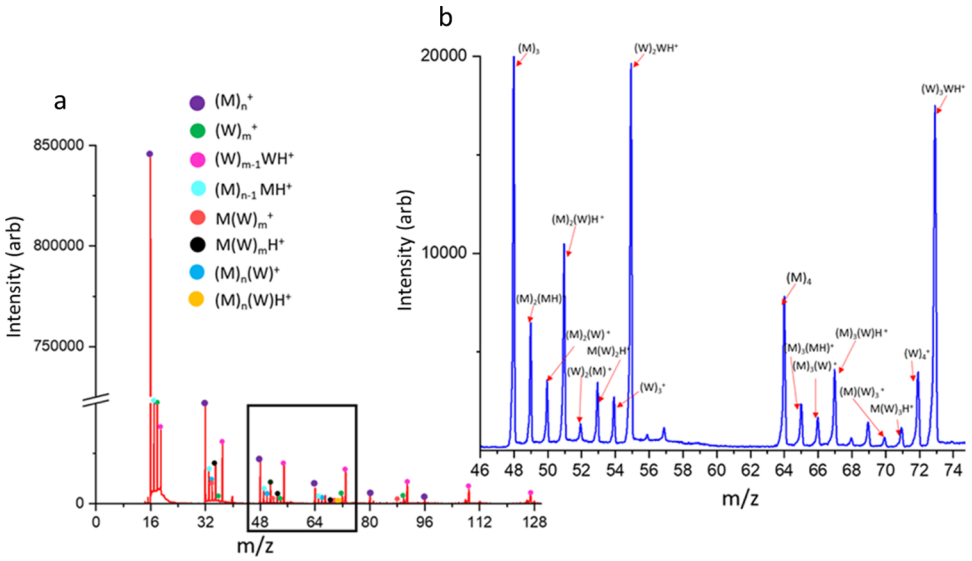

Figure 2. (a) The mass spectrum of methane-water clusters obtained at 65 psi backing pressure and 13 eV photon energy. The blue spectrum (b) shows an enlargement of the mass spectrum in the region of 46−74 m/z.

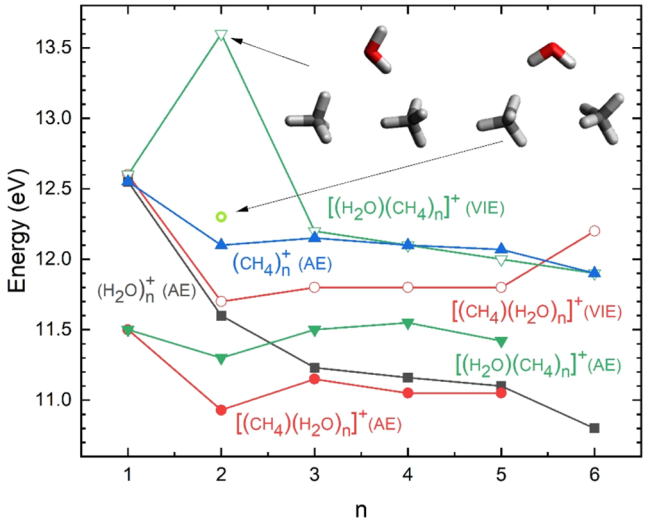

Figure 3. Experimental appearance energies (AE) of water clusters, water-dominated mixed clusters, methane clusters, and methane-dominated mixed clusters plotted up to 5 or 6 subunits. Also shown are calculated vertical ionization energies (VIE) for water-dominated mixed clusters, and methane-dominated mixed clusters. The calculated VIE of $H_2O(CH_4)_2$ derived from the structure in ref 34 is indicated by a thick-edged green circle. Also shown are the calculated structures of the neutral geometries for $H_2O(CH_4)_2$ calculated in this work and from ref 34.

$$(CH_4)_m + h\nu \rightarrow (CH_4)_m^+ + e^- \rightarrow (CH_4)_k^+ + e^- + (m-k)CH_4 \quad (1a)$$

$$(CH_4)_2 + h\nu \rightarrow [CH_3 - H - CH_4]^+ + e^- \rightarrow CH_5^+ + e^- + CH_3 \quad (1b)$$

The next main series in our mass spectra starts at m/z 17 and appears at every m/z 16 interval. Since we can safely assume we only produce singly ionized species, this would correspond to $[CH_5(CH_4)_n]^+$ $(n \geq 0)$ resulting from dissociative photoionization. A possible formation pathway to CH_5^+, which appears at m/z 17, starts from the long-range van der Waals-bound methane dimer. According to Zaag et al., after ionization of the dimer, a stable complex $[CH_3{-}H{-}CH_4]^+$ is formed, which then undergoes proton transfer to the CH_4 moiety and finally dissociates to yield the CH_5^+ cation (reaction 1b).[36] Similarly, larger clusters of the form $[CH_5(CH_4)_n]^+$ can be formed by ejection of the CH_3 moiety in the reaction described below.

Table 1. Experimental AE and Calculated VIE's in EV of Clusters (CH_4 and H_2O Mixed Clusters) Observed in this Study[a]

species	appearance energy (eV) ± 0.1	calculated vertical ionization energies (eV)
CH_4	12.6	
H_2O	12.6	
$CH_4(H_2O)$	11.5	12.6
$CH_4(H_2O)_2$	10.9	11.7
$CH_4(H_2O)_3$	11.2	11.8
$CH_4(H_2O)_4$	11.1	11.8
$CH_4(H_2O)_5$	11.0	11.8
$CH_4(H_2O)H$	11.5	
$CH_4(H_2O)_2H$	11.0	
$CH_4(H_2O)_3H$	11.1	
$CH_4(H_2O)_4H$	11.1	
$CH_4(H_2O)_5H$	11.0	
$H_2O(CH_4)_2$	11.3	13.6 (12.3)
$H_2O(CH_4)_3$	11.5	12.2
$H_2O(CH_4)_4$	11.5	12.1
$H_2O(CH_4)_5$	11.4	12.0
$H_2OH(CH_4)_2$	11.4	
$H_2OH(CH_4)_3$	11.6	
$H_2OH(CH_4)_4$	11.6	
$H_2OH(CH_4)_5$	11.5	
$CH_4(H_2O)_2H$	11.0	
$CH_4(H_2O)_3H$	11.1	
$CH_4(H_2O)_4H$	11.1	
$CH_4(H_2O)_5H$	11.0	

[a]The number in parentheses for the cluster $H_2O(CH_4)_2$ is calculated from the coordinates from Riera et al.[34]

https://doi.org/10.1021/acsearthspacechem.4c00151
ACS Earth Space Chem. 2024, 8, 1867−1876

$$(CH_4)_m + h\nu \rightarrow (CH_4)_m^+ + e^- \rightarrow (CH_4)_{k-1}CH_5^+ + e^- + (m-k)CH_4 + CH_3 \quad (2)$$

Herein, it is important to note that the ion−molecule reaction between CH_4^+ and CH_4 forming CH_3 and CH_5^+ is 6.2 kcal/mol exothermic, and generally, this type of ion-molecular reaction is barrierless in nature. This particular reaction has a bimolecular rate constant of 1.5 E^{-9} $molec^{-1}$ cm^3 s^{-1} and has a negative Arrhenius-type behavior which further indicates the presence of a prereactive complex.[37]

Similarly, in addition to pure methane clusters, we observed both water $[W_m]^+$ and protonated water clusters $[(W)_mH]^+$. As shown in Figure 2, the protonated water cluster intensity is higher than the water cluster of the same m except for $m = 1$, for all the conditions at 13 eV. This is expected at the high photon energy (i.e., ≥11 eV, the onset of the ionization of water clusters), where the excess energy results in proton transfer and dissociation and hence the formation of protonated water clusters. These results agree with previous VUV photoionization studies.[38−40]

Mixed Methane-Water Clusters. One significant finding in the methane-water system is the observation of mixed methane-water clusters. By adjusting a simple experimental parameter such as backing pressure, various-sized mixed clusters were produced, in stark contrast to previous attempts reported in the literature.[21,41] This is attributed to the combination of a higher backing pressure and expansion of the gas specifically through a 50 μm nozzle.

We can distinguish methane-water $[CH_4(W)_m]^+$ and protonated water−methane $[CH_4(W)_mH]^+$ clusters, with the latter displaying higher peak intensity in the mass spectrum than the former. The $[CH_4(W)_mH]^+$ series can be formed via the following photodissociative reaction.

$$CH_4(W)_m + h\nu \rightarrow [CH_4(W)_m]^+ + e^- \rightarrow [CH_4(W)_{m-1}H]^+ + e^- + OH \quad (3)$$

Following the rapid formation of protonated clusters through the above reaction, which contain excess energy, relatively slow water molecule evaporation occurs within the time-of-flight tube to release the excess energy from the parent cluster. Furthermore, at higher pressures, Ar can bind to these clusters, allowing for evaporative cooling of Ar to take place and effectively remove excess energy from the cluster. In such cases, this process quenches the OH elimination from the above reaction, resulting in the formation of unprotonated water−methane clusters $[CH_4(W)_m]^+$. We believe that a similar process can occur with methane when its concentration is high in the molecular beam. In such cases, additional methane molecules can bind to the structure, and evaporative cooling of these additional methane molecules can quench the OH elimination, resulting in the formation of unprotonated water−methane clusters.

We finally discuss the formation of water−methane clusters $[W(CH_4)_n]^+$, and water-protonated methane clusters $[(CH_4)_nWH]^+$, the latter displaying higher peak intensity in the mass spectrum than the former. One way of forming the water-protonated methane clusters is through the following photodissociative reaction which is similar to the reaction 3 we discussed above.

$$W(CH_4)_n + h\nu \rightarrow W(CH_4)_n^+ + e^- \rightarrow [(CH_4)_{n-1}WH]^+ + e^- + CH_3 \quad (4)$$

Proton transfer reactions such as these are also observed in acetaldehyde−water cluster systems.[42] Similar to the formation of methane-unprotonated water clusters $[CH_4(W_m)]^+$, Ar atoms can remove the excess energy of the clusters and quench CH_4 elimination, resulting in the formation of water−methane clusters $W(CH_4)_n$. However, it has been established in early work on methanol cluster photoionization that the successive evaporation of more than one molecule is less significant.[43]

In addition to the clusters discussed above, we observed other masses resulting from mixed clusters involving Ar and methane $(Ar(CH_4)_n)$, and clusters of the form $(CH_4)_nW_m$ and $[(CH_4)_nW_mH]^+$. The unlabeled peaks in Figure 2b may be attributed to these clusters. Ding et al.[35] also observed $[Ar(CH_4)]^+$ and $[Ar(CH_5)]^+$ in their study. The peaks appearing at mass 68 and 69 could be attributed to $[(CH_4)_2(H_2O)_2]^+$ and $[(CH_4)_2(H_2O)_2H]^+$, respectively. Although their presence cannot be conclusively confirmed solely through the detection of the m/z 68 and 69 peaks, the formation of these types of clusters is supported by the calculations of both Cao et al.[19] and Galashev et al.[18]

Interpretation of Photoionization Intensity Curves and Appearance Energies. The photoionization intensity curves for all cluster series seen in this study are shown in Figure S1 in the SI. Both methane and water have similar ionization energies of 12.6 eV and the photoionization intensity curves of the pure methane and water-related clusters exhibit fairly smooth and structureless curvature above the photoionization threshold. Following ionization, the clusters may accumulate excess internal energy, leading to energy-transfer processes and dissociative photoionization. This phenomenon can result in significant fragmentations within the clusters, leaving no noticeable features in the photoionization intensity curve.

The shape of the photoionization intensity curves of water is similar to previous studies by Belau et al.[44] and Ng et al.[45] The AEs' are also consistent with Belau et al.'s[44] study within 0.2 eV, except for the water monomer (see Table S1 in SI). This discrepancy may arise from potential contributions by dissociation of larger species present in the molecular beam, which have lower ionization onsets. Employing a higher backing pressure, similar to the approach reported by Shiromaru et al.,[46] results in an increase in the concentration of heterogeneous clusters, specifically of the type $Ar_x(H2O)_y$. It is plausible that the ionization energies of these clusters are somewhat lower, considering the bathochromic shift due to Ar in van der Waals clusters. The evaporation of Ar atoms from the photoionized cluster $Ar_x(H2O)_n$ could potentially alter the appearance energy of the water monomer channel. Additionally, the intensity of the water monomer drops after 12.9 eV, indicating the opening of other product channels starting from these larger species that may lead to the formation of different products besides water.

The experimental AEs' observed for methane clusters in our study are higher than those reported by Zaag et al. (see Table S1 in SI).[36] Similar to water-related clusters, the AE decreases as the cluster size increases. Note that this decrement is less pronounced in pure methane clusters than in pure water clusters. Compared with water, methane exhibits weaker

https://doi.org/10.1021/acsearthspacechem.4c00151
ACS Earth Space Chem. 2024, 8, 1867−1876

interactions, leading to lower contributions from heterogeneous clusters. This suggests that the influence of additional species on the observed AEs' is less pronounced in methane clusters compared to water clusters.

The gradual rise in the photoionization intensity curves of water, in comparison to methane clusters, further indicates that a larger proportion of small water clusters results from the fragmentation of other mixed clusters than those of small methane clusters. Moreover, as a general trend, the photoionization intensity curves of the methane-dominated mixed cluster align with its methane counterparts, while the water-dominated mixed cluster follows its water analogue.

Figure 4 shows the part of the photoionization intensity curve of water obtained with coexpanding methane (in Ar) at

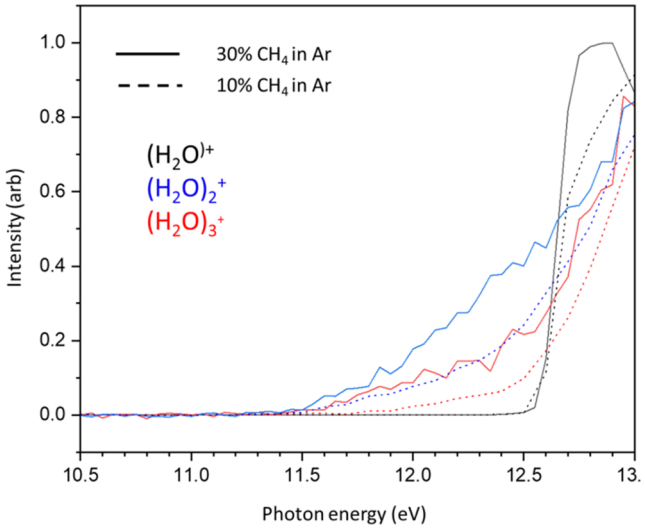

Figure 4. Photoionization intensity curves of the water monomer, dimer and trimer obtained at two different methane concentrations (10 and 30%). For better comparison, these photoionization intensity curves are normalized to the highest peak intensity (which is at 13.5 eV and not shown in the Figure) of each cluster.

two different methane concentrations (For clarity, the Figure 4 does not include data beyond 13 eV, where the signal for the clusters reaches its normalized peak value of 1), with all other experimental conditions held constant. At higher methane concentrations, the photoionization intensity curve has a steeper onset compared to lower methane concentrations. This suggests that at higher methane concentrations, more and larger methane-water clusters are formed, which have a lower AE, and these methane molecules dissociate from the water, ultimately resulting in the detection of water ions at lower photon energies. Therefore, an increased concentration of methane in the beam enhances the amount of evaporative cooling of the clusters, validating our argument regarding the formation of a number of (smaller) species via the dissociation of larger clusters upon ionization. In this context, we report on a theoretical TDDFT calculation of the electronic properties of a methane-water solution.[47] There it is reported that the first vertical excitation and ionization energies of methane are red-shifted by 0.45 and 0.87 eV, respectively, from the gas phase to solution. The latter number agrees reasonably well with what has been measured here, where we see a drop in the appearance energy of 1.1 eV in methane with the addition of water.

Observation of Methanol. A notable observation in this study is that methanol is formed in the photoionization of methane-water clusters. Previously observed in irradiation experiments involving bulk methane and water ices,[25,26] as discussed earlier, here methanol is observed in the smallest possible ice analogue under isolated conditions. Under normal conditions, the methanol mass (m/z = 32) overlaps with the signal obtained for the $(CH_4)_2$ cluster. To address this and to confirm the formation of methanol, we used deuterated water. Yet, under these conditions, the deuterated methanol (CH_3OD m/z 33) would coexist with the $CH_4CH_5^+$ cluster. Thus, to confirm methanol formation, we use both deuterated methane and deuterated water. Under fully deuterated conditions, a peak at m/z 36, potentially corresponding to methanol only, is observed. The mass spectrum showing the m/z 36 peak, at 12.5 eV and 60 psi backing pressure, is shown in Figure 5, with

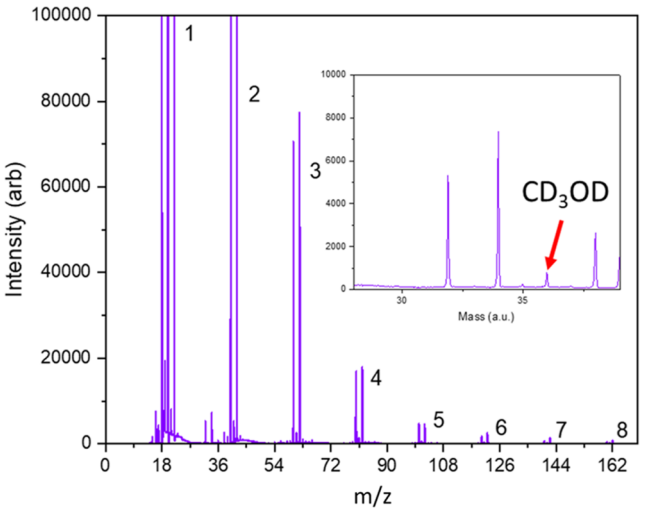

Figure 5. Mass spectra obtained using fully deuterated methane and water at 13 eV and 65 psi backing pressure conditions. The mass region of m/z 30−40 is zoomed in and included in the inset.

a zoom-in with the range m/z 28−40 in the inset. An alternative source of the peak at m/z 36 may be the water dimer, $(H_2O)_2$, which could potentially appear as a result of an impurity in the form of nondeuterated water. To address this possibility, various control mass spectra were obtained to eliminate contributions from certain species in the molecular beam. The peak at m/z 36 appears only when both methane and water components are present in the molecular beam and not with only one of the individual components present. Thus, these control experiments confirm that the m/z 36 peak most likely corresponds to methanol, formed via photoionization of deuterated methane and water clusters, rather than being attributed to $(H_2O)_2$. Additionally, we do not observe the protonated water dimer, which is usually present in higher quantities than the unprotonated water dimer.

As discussed earlier, the formation of methanol from methane and water in the solid phase occurs through either the reaction between methane and OH radicals or with $O(^1D)$ atoms.[25,26] There is evidence of such processes, albeit theoretically that such processes occur also in the gas phase.[48]

Chandra et al.[49] investigated the potential energy surface (PES) of methanol formation from $CH_4(H_2O)_6$ following ionization. Their calculations revealed that methanol formation occurs through two transition states. Initially, OH bond

https://doi.org/10.1021/acsearthspacechem.4c00151
ACS Earth Space Chem. 2024, 8, 1867−1876

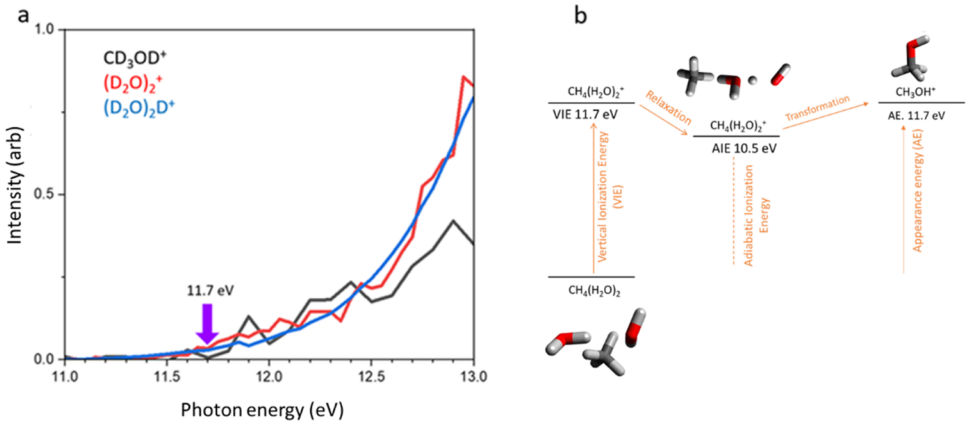

Figure 6. (a) The normalized photoionization intensity curves of deuterated methanol, $(D_2O)_2^+$ and $(D_2O)_2D^+$. The appearance energy of methanol is indicated by an arrow and the number above it. (b) Calculated vertical ionization energy and adiabatic ionization energy of the $CH_4(H_2O)_2$ cluster. The appearance energy for methanol is an experimental determination in this work.

dissociation occurs in one of the water molecules of the cluster within 50 fs. This is essentially described by reaction 3, which we identified for the formation of $[CH_4(W)_mH]^+$. Subsequently, C−H bond dissociation occurs, followed by the formation of the C−O bond. Here, we provide experimental evidence that methanol could indeed be formed following photoionization of methane-water clusters, not only with the detection of methanol as a product but also by the identification of intermediates. As reported by Hendrix et al.,[50] recently, quantum chemical calculations show that the binding energies of small charged clusters involving water and other small molecules, such as $CH_3^+(H_2O)_n$ and $NH_2^+(H_2O)_n$, are higher than those of neutral clusters. For certain species with higher binding energies, these clusters can go one step further and react spontaneously with the members of the water cluster to form new compounds. These are in agreement with Woon et al.[51] who performed theoretical calculations on the spontaneous formation of a neutral methanol molecule and H_3O^+ upon adding a methyl ion to a $(H_2O)_{17}$ water cluster. Nakai et al.[52] recently confirmed experimentally this postulation by reacting low-energy methyl cations with amorphous solid water at low temperatures (12−60 K) and observing methanol formation. Ab initio molecular dynamics simulations performed by the same group[52] on a methyl cation reacting with a $(H_2O)_{47}$ cluster showed that methanol formation was spontaneous and did not depend on the initial configuration of the complex.

Analysis of the AE of the methanol species provides more evidence for the origin of this species and the pathways involved in its formation. Figure 6a shows the part of the normalized photoionization intensity curves for the m/z 36 mass plotted with $(D_2O)_2$ and $(D_2O)_2D^+$ measured in the same experiment in the range from 11 to 13 eV (For clarity, the Figure 6 does not include data beyond 13 eV, where the signal for the clusters reaches its normalized peak value of 1). Both the AE of 11.7 eV and the shape in those curves, when compared with methanol, show strong similarity. This is reminiscent of previous work performed on the VUV photoionization dynamics in naphthalene-water clusters and dimethyl uracil water clusters. Xu et al.[53] have observed OH addition to naphthalene in naphthalene-water clusters upon ionization of a water subcluster bound to naphthalene. This subwater cluster can then undergo proton transfer to the naphthalene moiety, resulting in the formation of protonated naphthalene clusters while eliminating OH radicals. In certain cases, however, the OH radicals remain in the vicinity of the main cluster and react with naphthalene to form hydroxynapthalene. Khistyaev et al.[54] observed similar behavior in proton transfer reactions in nucleobases clustered to water. From an analysis of the photoionization intensity curves and theoretical calculations, it was inferred that the mechanism involves initial vertical ionization to the 3A″ state of water at around 11.2 eV and subsequent proton transfer. Very recently, Salbaing et al.[55] have seen similar results for intracluster reactions, specifically in protonated methanol clusters where a water molecule is eliminated from the protonated methanol clusters during collisional relaxation. They have observed that this reaction is cluster dependent and occurs only in small methanol clusters. We expect a similar mechanism involving proton transfer to be at play within methane-water clusters.

To verify this, DFT calculations were performed to calculate the vertical ionization energies (VIE) and adiabatic ionization energies (AIE) of the $CH_4(H_2O)_2$ cluster. We specifically choose small water clusters because of our previous observation of small naphthalene-water clusters potentially influencing the formation of hydroxy naphthalene.[53] As illustrated in Figure 6b, vertical ionization of $CH_4(H_2O)_2$ occurs at approximately 11.7 eV. This vertical ionization leads to a nonstationary nuclear configuration of the cluster, which evolves to an adiabatic ion state about 10.5 eV higher than the neutral cluster. By subtracting the AE of methanol (11.7 eV) from the AIE, we find that approximately 1.2 eV of energy remains within the system. This excess energy governs the transformation of excited-state $[CH_4(H_2O)_2]^+$ to a methanol ion. As discussed earlier, the calculations by Chandra et al.[49] support the formation of methanol from $CH_4(H_2O)_6$ via two transition states. One pathway involves proton transfer between water molecules, while the other involves proton transfer between CH_4 and water. Ultimately, molecular hydrogen abstraction occurs to form the CO bond. These transition states exhibit submerged barriers compared to the VIE of the $CH_4(H_2O)_6$ cluster, which is approximately 11 eV. For the $(CH_4)(H_2O)_n$ clusters we obtained, comparable VIEs are observed, suggesting a similar mechanism may occur, in addition to the mechanisms suggested by Xu et al.[53] and Khistyaev et al.[54]

Our unique method of employing synchrotron-based tunable VUV photoionization allows us to both prepare and

https://doi.org/10.1021/acsearthspacechem.4c00151
ACS Earth Space Chem. 2024, 8, 1867−1876

probe the rich chemistry that occurs in these methane-water clusters. As discussed in the Introduction, these results have implications in astrochemistry particularly for the photoprocessing of ices and subsequent formation of complex organic molecules which could be the precursors of biotic systems.[9] There are two studies in the literature,[25,27] where IR spectroscopy was used to probe the VUV photochemistry of methane-water ices, however, in both cases, it was broadband VUV light from a lamp which was filtered by a MgF_2 window, thus effectively removing light above 10.8 eV. As shown in our work, it is important to probe in the region above this cutoff, and use mass selective detection to be able to tease out the complex chemical processes that are proposed to occur in space, for instance, methanol formation on the Kuiper Belt object Arrokoth.[28,56] One could argue that our clusters are not reflective of an icy environment; however, we can show evidence from the literature that indeed, that is not the case. There is a mass spectrum of 0.01 ML of water and 0.2 ML of methane coadsorbed on solid Ne (5.9 K) generated by photodesorption at 70 eV by light generated with a laser plasma VUV light source[57] which is similar to our results recorded at 12.5 eV (see Figure S3 in SI). In that work, the authors argue that the presence of water is essential for the observation of desorption supporting our assertion that methanol formation in methane-water clusters is mediated by excitation in the water cluster. Another indirect evidence comes from a theoretical study of hydrogen bonds in methane-water clusters. In that work,[21] the authors studied the CH_4-$(H_2O)_{12}$ cluster and performed Gibbs energy analysis at several temperatures, and suggested that compact water clusters can be formed that interacts with an external methane molecule as opposed to the typical clathrate structures proposed. Studies were performed at 3 temperatures, 100, 200, and 300 K, and it was noted that there were a number of conformers that are populated both at 100 and 200 K temperatures, and this lies within the vibrational energy content of our molecular beams.

CONCLUSIONS

We observed a series of methane-water clusters using VUV photoionization. Our experiment demonstrates how slight changes in experimental conditions can significantly affect the cluster distribution. Previous theoretical and experimental research on various cluster systems has brought to light the potential for rich chemistry occurring within clusters upon ionization. The methane−water system stands out as an excellent example, wherein cluster rearrangement facilitates the formation of new molecular species after photoionization. Our study presents compelling evidence for the gas-phase formation of methanol in VUV photoionized methane-water clusters, thereby confirming previous theoretical work.[49] This study further demonstrates that small clusters mimic astrochemical ices, and the photoionization of these small clusters provides valuable insights into the pathways of molecular formation in astrochemical ices.

ASSOCIATED CONTENT

Supporting Information

The Supporting Information is available free of charge at https://pubs.acs.org/doi/10.1021/acsearthspacechem.4c00151.

Photoionization intensity curves for the clusters detected in this work. The optimized structures of $CH_4(H_2O)_n$; $[(CH_4)(H_2O)_n]^+$; $H_2O(CH_4)_n$; $[H_2O(CH_4)_n]^+$; $[CH_5(CH_4)_n]^+$; $[CH_4(H_2O)_nH]^+$;$[H_3O(CH_4)_n]^+$. Comparison of mass spectra recorded at 12.5 eV photon energy to that measured from desorption of ions from a water−methane monolayer at 5.6 K matrix irradiated with 70 eV photons, the appearance energy of water clusters and methane clusters in this study compared with previous experiments (PDF)

Cartesian coordinates used to calculate the optimized structures reported in this work (ZIP)

AUTHOR INFORMATION

Corresponding Author

Musahid Ahmed − *Chemical Sciences Division, Lawrence Berkeley National Laboratory, Berkeley, California 94720, United States;* orcid.org/0000-0003-1216-673X; Email: mahmed@lbl.gov

Authors

Nureshan Dias − *Chemical Sciences Division, Lawrence Berkeley National Laboratory, Berkeley, California 94720, United States;* orcid.org/0000-0002-4518-0901

Alexander K. Lemmens − *Chemical Sciences Division, Lawrence Berkeley National Laboratory, Berkeley, California 94720, United States;* orcid.org/0000-0002-2474-2346

Anna Wannenmacher − *Chemical Sciences Division, Lawrence Berkeley National Laboratory, Berkeley, California 94720, United States*

Complete contact information is available at: https://pubs.acs.org/10.1021/acsearthspacechem.4c00151

Notes

The authors declare no competing financial interest.

ACKNOWLEDGMENTS

This work is supported by the Gas Phase Chemical Physics Program, in the Chemical Sciences Geosciences and Biosciences Division of the Office of Basic Energy Sciences of the U.S. Department of Energy under Contract No. DE-AC02-05CH11231 and the U.S. Department of Energy, Office of Science, Office of Workforce Development for Teachers and Scientists, Office of Science Graduate Student Research (SCGSR) program (Contract No. DE-SC0014664). This research used resources from the Advanced Light Source, which is a DOE Office of Science User Facility under Contract No. DE-AC02-05CH11231.

REFERENCES

(1) Yung, Y. L.; Chen, P.; Nealson, K.; Atreya, S.; Beckett, P.; Blank, J. G.; Ehlmann, B.; Eiler, J.; Etiope, G.; Ferry, J. G.; et al. Methane on Mars and habitability: challenges and responses. *Astrobiology* **2018**, *18* (10), 1221−1242.

(2) Novak, R. E.; Mumma, M. J.; Villanueva, G. L. Measurement of the isotopic signatures of water on Mars; Implications for studying methane. *Planet. Space Sci.* **2011**, *59* (2−3), 163−168.

(3) Fonti, S.; Marzo, G. A. Mapping the methane on Mars. *Astron. Astrophys.* **2010**, *512*, A51.

(4) Cruikshank, D. P.; Apt, J. Methane on Triton: Physical state and distribution. *Icarus* **1984**, *58* (2), 306−311.

(5) Cruikshank, D. P.; Schmitt, B.; Roush, T. L.; Owen, T. C.; Quirico, E.; Geballe, T. R.; de Bergh, C.; Bartholomew, M. J.; Dalle Ore, C. M.; Douté, S. Water ice on Triton. *Icarus* **2000**, *147* (1), 309−316.

(6) Tegler, S. C.; Grundy, W. M.; Olkin, C. B.; Young, L. A.; Romanishin, W.; Cornelison, D. M.; Khodadadkouchaki, R. Ice mineralogy across and into the surfaces of Pluto, Triton, and Eris. *Astrophys. J.* **2012**, *751* (1), 76.
(7) Lunine, J. I. The atmospheres of Uranus and Neptune. *Annu. Rev. Astron. Astrophys.* **1993**, *31* (1), 217−263.
(8) Moses, J. I.; Cavalié, T.; Fletcher, L. N.; Roman, M. T. Atmospheric chemistry on Uranus and Neptune. *Philos. Trans. R. Soc., A* **2020**, *378* (2187), No. 20190477.
(9) Öberg, K. I. Photochemistry and astrochemistry: Photochemical pathways to interstellar complex organic molecules. *Chem. Rev.* **2016**, *116* (17), 9631−9663.
(10) Wolfire, M. G.; Vallini, L.; Chevance, M. Photodissociation and X-Ray-Dominated Regions. *Annu. Rev. Astron. Astrophys.* **2022**, *60* (1), 247−318.
(11) Sloan, E. D., Jr Fundamental principles and applications of natural gas hydrates. *Nature* **2003**, *426* (6964), 353−359.
(12) Ripmeester, J. A.; Tse, J. S.; Ratcliffe, C. I.; Powell, B. M. A new clathrate hydrate structure. *Nature* **1987**, *325* (6100), 135−136, DOI: 10.1038/325135a0.
(13) Buffett, B. A. Clathrate hydrates. *Annu. Rev. Earth Planet. Sci.* **2000**, *28* (1), 477−507.
(14) Mousis, O.; Chassefière, E.; Holm, N. G.; Bouquet, A.; Waite, J. H.; Geppert, W. D.; Picaud, S.; Aikawa, Y.; Ali-Dib, M.; Charlou, J.-L.; Rousselot, P. Methane clathrates in the solar system. *Astrobiology* **2015**, *15* (4), 308−326.
(15) Galashev, A. E. Structural changes in water clusters during methane adsorption. *Colloid J.* **2014**, *76*, 300−307.
(16) Galashev, A. E. Structure of water clusters with captured methane molecules. *Russ. J. Phys. Chem. B* **2014**, *8*, 793−800.
(17) Galashev, A. E.; Rakhmanova, O. R. Computer study of methane adsorption by water clusters. *High Temp.* **2013**, *51* (3), 369−376.
(18) Galashev, A. E.; Chukanov, V. N.; Novruzov, A. N.; Novruzova, O. A. Molecular-dynamic calculation of spectral characteristics of absorption of infrared radiation by $(H_2O)_j$ and $(CH_4)_i$ $(H_2O)_n$ clusters. *High Temp.* **2006**, *44*, 364−372.
(19) Cao, X.; Su, Y.; Liu, Y.; Zhao, J.; Liu, C. Storage capacity and vibration frequencies of guest molecules in CH_4 and CO_2 hydrates by first-principles calculations. *J. Phys. Chem. A* **2014**, *118* (1), 215−222.
(20) Ruckenstein, E.; Shulgin, I. L.; Tilson, J. L. The structure of dilute clusters of methane and water by ab initio quantum mechanical calculations. *J. Phys. Chem. A* **2003**, *107* (13), 2289−2295.
(21) Salazar-Cano, J.-R.; Guevara-García, A.; Vargas, R.; Restrepo, A.; Garza, J. Hydrogen bonds in methane−water clusters. *Phys. Chem. Chem. Phys.* **2016**, *18* (34), 23508−23515.
(22) Olesen, S. G.; Gausco, T. L.; Weddle, G. H.; Hammerum, S.; Johnson, M. A. Vibrational predissociation spectra of the Ar-tagged $[CH_4 \cdot H_3O^+]$ binary complex: spectroscopic signature of hydrogen bonding to an alkane. *Mol. Phys.* **2010**, *108* (7−9), 1191−1197.
(23) Mizuse, K.; Fujii, A. Infrared photodissociation spectroscopy of $H^{(+)}(H_2O)_6.M_{(m)}$ (M = Ne, Ar, Kr, Xe, H_2, N_2, and CH_4): messenger-dependent balance between $H_3O^{(+)}$ and $H_5O_2^{(+)}$ core isomers. *Phys. Chem. Chem. Phys.* **2011**, *13* (15), 7129−7135.
(24) McCoy, A. B.; Guasco, T. L.; Leavitt, C. M.; Olesen, S. G.; Johnson, M. A. Vibrational manifestations of strong non-Condon effects in the $H_3O^{(+)}.X_3$ (X = Ar, N_2, CH_4, H_2O) complexes: a possible explanation for the intensity in the "association band" in the vibrational spectrum of water. *Phys. Chem. Chem. Phys.* **2012**, *14* (20), 7205−7214.
(25) Krim, L.; Jonusas, M. VUV Photolysis of CH_4−H_2O mixture in methane-rich ices: Formation of large complex organic molecules in astronomical environments. *Low Temp. Phys.* **2019**, *45* (6), 606−614.
(26) Wada, A.; Mochizuki, N.; Hiraoka, K. Methanol formation from electron-irradiated mixed H2O/CH4 ice at 10 K. *Astrophys. J.* **2006**, *644* (1), 300.
(27) Hodyss, R.; Johnson, P. V.; Stern, J. V.; Goguen, J. D.; Kanik, I. Photochemistry of methane−water ices. *Icarus* **2009**, *200* (1), 338−342.
(28) Grundy, W. M.; Bird, M. K.; Britt, D. T.; Cook, J. C.; Cruikshank, D. P.; Howett, C. J. A.; Krijt, S.; Linscott, I. R.; Olkin, C. B.; Parker, A. H.; et al. Color, composition, and thermal environment of Kuiper Belt object (486958) Arrokoth. *Science* **2020**, *367* (6481), No. eaay3705.
(29) Nicolas, C.; Shu, J.; Peterka, D. S.; Hochlaf, M.; Poisson, L.; Leone, S. R.; Ahmed, M. Vacuum ultraviolet photoionization of C_3. *J. Am. Chem. Soc.* **2006**, *128* (1), 220−226.
(30) Belau, L.; Wilson, K. R.; Leone, S. R.; Ahmed, M. Vacuum ultraviolet (VUV) photoionization of small water clusters. *J. Phys. Chem. A* **2007**, *111* (40), 10075−10083.
(31) Pracht, P.; Bohle, F.; Grimme, S. Automated exploration of the low-energy chemical space with fast quantum chemical methods. *Phys. Chem. Chem. Phys.* **2020**, *22* (14), 7169−7192.
(32) Shao, Y.; Gan, Z.; Epifanovsky, E.; Gilbert, A. T. B.; Wormit, M.; Kussmann, J.; Lange, A. W.; Behn, A.; Deng, J.; Feng, X.; et al. Advances in molecular quantum chemistry contained in the Q-Chem 4 program package. *Mol. Phys.* **2015**, *113* (2), 184−215.
(33) Mardirossian, N.; Head-Gordon, M. ωB97X-V: A 10-parameter, range-separated hybrid, generalized gradient approximation density functional with nonlocal correlation, designed by a survival-of-the-fittest strategy. *Phys. Chem. Chem. Phys.* **2014**, *16* (21), 9904−9924.
(34) Riera, M.; Hirales, A.; Ghosh, R.; Paesani, F. Data-Driven Many-Body Models with Chemical Accuracy for CH_4/H_2O Mixtures. *J. Phys. Chem. B* **2020**, *124* (49), 11207−11221.
(35) Ding, A.; Cassidy, R. A.; Futrell, J. H.; Cordis, L. Ion−molecule reactions within methane clusters initiated by photoionization. *J. Phys. Chem. A* **1987**, *91* (10), 2562−2568.
(36) Zaag, A. S.; Yazidi, O.; Jaidane, N. E.; Ross, M. W.; Castleman, A. W., Jr; Al Mogren, M. M.; Linguerri, R.; Hochlaf, M. Structure, reactivity, and fragmentation of small multi-charged methane clusters. *J. Phys. Chem. A* **2016**, *120* (10), 1669−1676.
(37) Anicich, V. G. Evaluated bimolecular ion−molecule gas phase kinetics of positive ions for use in modeling planetary atmospheres, cometary comae, and interstellar clouds. *J. Phys. Chem. Ref. Data* **1993**, *22* (6), 1469−1569.
(38) Golan, A.; Ahmed, M. Ionization of water clusters mediated by exciton energy transfer from argon clusters. *J. Phys. Chem. Lett.* **2012**, *3* (4), 458−462.
(39) Shinohara, H.; Nishi, N.; Washida, N. Photoionization of water clusters at 11.83 eV: Observation of unprotonated cluster ions $(H_2O)^+$ n (2≤ n≤ 10). *J. Chem. Phys.* **1986**, *84* (10), 5561−5567.
(40) Mackie, C. J.; Lu, W.; Liang, J.; Kostko, O.; Bandyopadhyay, B.; Gupta, I.; Ahmed, M.; Head-Gordon, M. Magic Numbers and Stabilities of Photoionized Water Clusters: Computational and Experimental Characterization of the Nanosolvated Hydronium Ion. *J. Phys. Chem. A* **2023**, *127* (29), 5999−6011.
(41) Ghosh, J.; Vishwakarma, G.; Kumar, R.; Pradeep, T. Formation and Transformation of Clathrate Hydrates under Interstellar Conditions. *Acc. Chem. Res.* **2023**, *56* (16), 2241−2252.
(42) Kostko, O.; Troy, T. P.; Bandyopadhyay, B.; Ahmed, M. Proton transfer in acetaldehyde−water clusters mediated by a single water molecule. *Phys. Chem. Chem. Phys.* **2016**, *18* (36), 25569−25573.
(43) Fu, H. B.; Hu, Y. J.; Bernstein, E. R. IR+ vacuum ultraviolet (118 nm) nonresonant ionization spectroscopy of methanol monomers and clusters: Neutral cluster distribution and size-specific detection of the OH stretch vibrations. *J. Chem. Phys.* **2006**, *124* (2), No. 024302, DOI: 10.1063/1.2141951.
(44) Belau, L.; Wheeler, S. E.; Ticknor, B. W.; Ahmed, M.; Leone, S. R.; Allen, W. D.; Schaefer, H. F.; Duncan, M. A. Ionization thresholds of small carbon clusters: tunable VUV experiments and theory. *J. Am. Chem. Soc.* **2007**, *129* (33), 10229−10243.
(45) Ng, C. Y.; Trevor, D. J.; Tiedemann, P. W.; Ceyer, S. T.; Kronebusch, P. L.; Mahan, B. H.; Lee, Y.-T. Photoionization of dimeric polyatomic molecules: Proton affinities of H2O and HF. *J. Chem. Phys.* **1977**, *67* (9), 4235−4237.
(46) Shiromaru, H.; Shinohara, H.; Washida, N.; Yoo, H.-S.; Kimura, K. Synchrotron radiation measurements of appearance

potentials for $(H_2O)_2^+$,$(H_2O)_3^+$,$(H_2O)_2H^+$ and $(H_2O)_3H^+$ in supersonic jets. *Chem. Phys. Lett.* **1987**, *141* (1−2), 7−11.
(47) Mateus, M. P. S.; Galamba, N.; Cabral, B. J. C.; Coutinho, K.; Canuto, S. Electronic properties of a methane−water solution. *Chem. Phys. Lett.* **2011**, *506* (4−6), 183−189.
(48) Chang, A. H. H.; Lin, S. H. A theoretical study of the O (^{1}D)+ CH_4 reaction II. *Chem. Phys. Lett.* **2004**, *384* (4−6), 229−235.
(49) Chandra, S. Theoretical investigation of methanol formation from methane water-ice cluster following ionization. *Mol. Astrophys.* **2019**, *16*, No. 100045.
(50) Hendrix, J.; Bera, P. P.; Lee, T. J.; Head-Gordon, M. Quantum chemical exploration of the binding motifs and binding energies of neutral molecules, radicals and ions with small water clusters: characterisation and astrochemical implications. *Mol. Phys.* **2024**, *122* (7−8), No. e2252100.
(51) Woon, D. E. Ion−IcE Astrochemistry: Barrierless low-energy deposition pathways to HCOOH, CH_3OH, and CO_2 on icy grain mantles from precursor cations. *Astrophys. J.* **2011**, *728* (1), 44.
(52) Nakai, Y.; Sameera, W. M. C.; Furuya, K.; Hidaka, H.; Ishibashi, A.; Watanabe, N. Methanol Formation through Reaction of Low-energy CH_3^+ Ions with an Amorphous Solid Water Surface at Low Temperature. *Astrophys. J.* **2023**, *953* (2), 162.
(53) Xu, B.; Stein, T.; Ablikim, U.; Jiang, L.; Hendrix, J.; Head-Gordon, M.; Ahmed, M. Probing solvation and reactivity in ionized polycyclic aromatic hydrocarbon−water clusters with photoionization mass spectrometry and electronic structure calculations. *Faraday Discuss.* **2019**, *217*, 414−433.
(54) Khistyaev, K.; Golan, A.; Bravaya, K. B.; Orms, N.; Krylov, A. I.; Ahmed, M. Proton transfer in nucleobases is mediated by water. *J. Phys. Chem. A* **2013**, *117* (31), 6789−6797.
(55) Salbaing, T.; Comte, D.; Lavy, L.; Lissillour, H.; Ospina, L. P.; Bertier, P.; Feketeová, L.; Calvo, F.; Farizon, B.; Farizon, M.; Märk, T. Water molecule elimination from the protonated methanol dimer ion—An example of a size-selective intracluster reaction. *J. Chem. Phys.* **2024**, *160* (9), No. 094301, DOI: 10.1063/5.0190182.
(56) McKinnon, W. B.; Richardson, D. C.; Marohnic, J. C.; Keane, J. T.; Grundy, W. M.; Hamilton, D. P.; Nesvorný, D.; Umurhan, O. M.; Lauer, T. R.; Singer, K. N.; et al. The solar nebula origin of (486958) Arrokoth, a primordial contact binary in the Kuiper Belt. *Science* **2020**, *367* (6481), No. eaay6620.
(57) Arakawa, I.; Matsumoto, D.; Takekuma, S.; Tamura, R.; Miura, T. Photo-stimulated desorption from water and methane clusters on the surface of solid neon. *Low Temp. Phys.* **2012**, *38* (8), 745−748.